Near-unity angular anisotropy of circularly polarized luminescence from microspheres of monodispersed chiral conjugated polymer

Journal:	*ChemComm*
Manuscript ID	CC-COM-03-2024-001428.R1
Article Type:	Communication

Data availability

The data supporting this article have been included as part of the Supplementary Information.

COMMUNICATION

Near-unity angular anisotropy of circularly polarized luminescence from microspheres of monodispersed chiral conjugated polymer

Received 00th January 20xx,
Accepted 00th January 20xx

DOI: 10.1039/x0xx00000x

Sota Nakayama, [a] Hiroshi Yamagishi, *[a] Osamu Oki, [a] Soh Kushida, [a] Junhui Chen, [a] Junpei Kuwabara, [a] Takaki Kanbara, [a] Wijak Yospanya, [b] Reiko Oda, [c, b] and Yohei Yamamoto *[a]

A microsphere, assembled from a chiral π-conjugated polymer with narrow polydispersity, features a well-organized twisted-bipolar structure and exhibits highly biased circularly polarized luminescence (CPL). The CPL emitted toward the equatorial direction is 61-fold greater than that emitted along the zenith direction, which is the highest anisotropy among existing microscopic CPL emitters.

Circularly Polarized Luminescence (CPL) is an attractive class of light for realizing advanced optoelectrical devices such as three dimensional displays[1–2], biosensors[3–5], and optical cryptography[6–7]. CPL emitters with a dimension less than several micrometers are particularly promising because they can be integrated and accumulated in a large scale and are applicable for the fabrication of advanced displays and sensors[8–17]. The bias of CPL, namely, dissymmetry factor (g_{lum}) of the luminescence radiated from such minute CPL emitters has been the major focus in the field of organic photonics and has been improved by integrating chiral structures into the micro-emitters. Small droplets consisting of liquid crystals (LC) are the most attractive materials platform in this field[18–21]. In parallel to the miniaturization, elaborating the angular anisotropy of the CPL has become an emerging target for further advancing the optoelectronic device applications[22–24], although its realization remains challenging.

We recently reported that a chiral π-conjugated polymer, poly(9,9'-bis((*S*)-3,7-dimethyloctyl)-2,7-fluorene-*alt*-benzothiadiazole) ((*S*,*S*)-PFBT, Fig. 1a), and its enantiomeric counterpart, ((*R*,*R*)-PFBT) self-assembled into well-defined microspheres (**MS**s) with an average diameter of 3.8 μm, featuring twisted bipolar (TB) molecular order at the interior, whose handedness depends on the point chirality of PFBT[22]. Notably, **MS** emitted intense CPL with the $|g_{\mathrm{lum}}|$ value as high as 0.5 along the horizontal direction while $|g_{\mathrm{lum}}|$ decreased to 0.2 along the zenith direction. The angular anisotropy reported therein was unprecedentedly high in comparison to those reported for the existing CPL emitters.

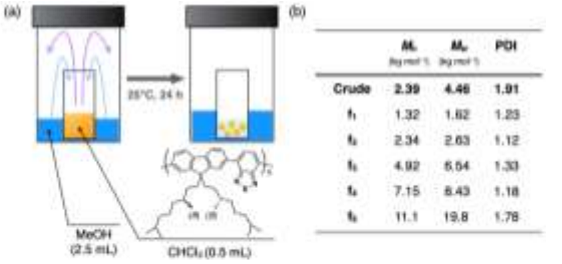

	M_n (kg mol⁻¹)	M_w (kg mol⁻¹)	PDI
Crude	**2.39**	**4.46**	**1.91**
f_1	1.32	1.62	1.23
f_2	2.34	2.63	1.12
f_3	4.92	6.54	1.33
f_4	7.15	8.43	1.18
f_5	11.1	19.8	1.78

Fig. 1 (a) A schematic representation of a procedure for the self-assembly of **MS** from PFBT by vapor diffusion method. (b) Tabular summary of the number- and weight-average molecular weight (M_n and M_w, respectively) of PFBT before (crude) and after fractionation ($\mathbf{f}_1$–$\mathbf{f}_5$).

However, the anisotropy did not match well with the value expected from the molecular order of the twisted bipolar arrangement. Ideally, the cholesteric order aligns toward the equatorial direction to the polar axis, therefore CPL should not be emitted toward the zenith direction. We attributed this to the large polydispersity of PFBT featuring polydispersity index (PDI) of 2.20. In the present study, we prepared **MS** from enantiomerically pure PFBT with a series of number-average molecular weight (M_n) and a smaller PDI. As a result, we found that **MS** with a certain molecular weight emitted CPL with significantly high angular anisotropy with the degree of anisotropy of almost unity. We further investigated the mechanism on how the TB order formed in **MS** and revealed that the thermal stability of the mesophase played an important role for the structural integrity of **MS**.

(*S*,*S*)-PFBT was synthesized according to our previous report[25]. We fractionated the resulting polymer by size

---

[a.] *Department of Materials Science, Institute of Pure and Applied Sciences, and Tsukuba Research Center for Energy Materials Science (TREMS), University of Tsukuba, 1-1-1 Tennodai, Tsukuba, Ibaraki 305-8573, Japan.*
[b.] *Advanced Institute of Material Research (AIMR), Tohoku University 2-1-1 Katahira, Aoba, Sendai, Miyagi, 980-8577, Japan.*
[c.] *University of Bordeaux, CNRS, Bordeaux INP, CBMN, UMR 5248, F-33600 Pessac, France*

† Electronic Supplementary Information (ESI) available: [details of any supplementary information available should be included here]. See DOI: 10.1039/x0xx00000x

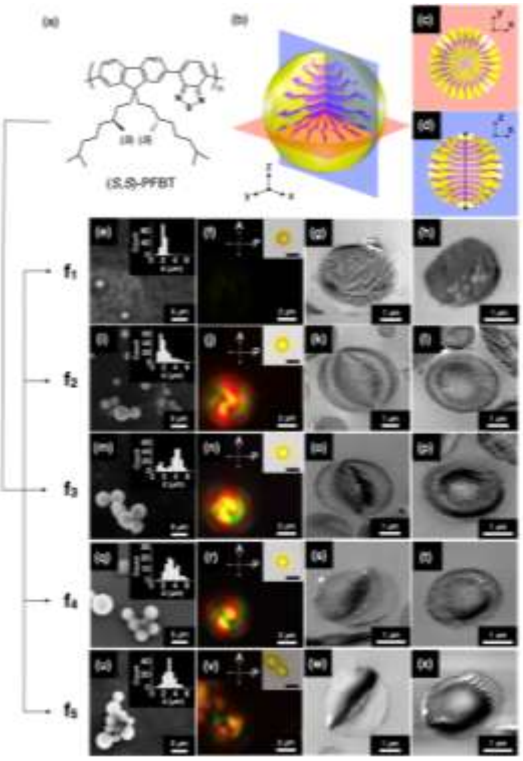

Fig. 2 (a) Molecular structure of (*S*,*S*)-PFBT. (b-d) Schematic representation of the TB molecular arrangement in **MS** and its cross-sectional views at the y–z (c) and x–z (d) planes. (e, i, m, q, u) SEM micrographs (insets are the histograms of the diameter) and (f, j, n, r, v) POM micrographs (insets are the corresponding OM images, scale bars: 4 μm) of the fractions of (*S*,*S*)-PFBT. (g-h, k-l, o-p, s-t, w-x) TEM micrographs of sliced pieces of **(*S*,*S*)-MS**.

exclusion chromatography (SEC) and obtained five fractions of (*S*,*S*)-PFBT (named **f**$_1$–**f**$_5$, respectively) with M_n ranging from 1.3 to 11 kg mol^{-1} and PDI less than 1.78 (Figs. 1b and S1–3). All the fractions displayed similar photoluminescence (PL) band at 534–540 nm in CHCl$_3$ and 540–558 nm in the cast film (Fig. S4). The microspherical particles of (*S*,*S*)-PFBT ((*S*,*S*)-**MS**) were assembled from each fraction by slowly diffusing MeOH vapour into the CHCl$_3$ solution of PFBT at 25°C[22, 26]. After the incubation, (*S*,*S*)-PFBT precipitated as yellow powder at the bottom of the vial in 24 h (Fig. 1a).

The microscopic morphology of the precipitates was visualized by scanning electron, optical and polarized optical microscopies (SEM, OM and POM, respectively). Every precipitate obtained from **f**$_1$–**f**$_5$ consisted of microspherical particles (Fig. 2e, i, m, q, u), while the amount of the particles was drastically small for **f**$_1$ in comparison to the other four fractions. The surface of the microspheres was smooth except those yielded from **f**$_5$ (Fig. 2u). OM images of the precipitates showed consistent results in terms of morphology and surface smoothness (Fig. S5).

The textures of **MS** observed with POM showed a clear dependence on M_n of PFBT. The POM textures were examined by selecting **MS** with a diameter in a range from 4.0 to 4.5 µm to eliminate the effect of the size. **MS** assembled from **f**$_1$ ((*S,S*)-**MS**$_{\mathbf{f1}}$) appeared mostly dark in POM, indicating the amorphous aggregation of the polymer chains of PFBT inside (*S,S*)-**MS**$_{\mathbf{f1}}$ (Fig. 2f) as is usual for most particles made of polymers (Fig. S6) [26–29]. **MS**s obtained from other four fractions ((*S,S*)-**MS**$_{\mathbf{f2–f5}}$) exhibited counterclockwise spiral texture (Fig. 2j, n, r, v), characteristic of the TB phase. The handedness of the spiral was the same over the particles observed. The spiral texture was explicit with (*S,S*)-**MS**$_{\mathbf{f2}}$ to (*S,S*)-**MS**$_{\mathbf{f4}}$, while it was incomplete with (*S,S*)-**MS**$_{\mathbf{f5}}$. Microspheres assembled from (*R,R*)-PFBT showed analogous spiral texture but the handedness was opposite (clockwise, Fig. S7), corroborating that the handedness of the twisted bipolar phase in **MS** was defined by the point chirality of PFBT.

The TB molecular arrangement was precisely verified by slicing (*S,S*)-**MS** into thin film and by observing the film with transmission electron microscopy (TEM). (*S,S*)-**MS**s were embedded in an epoxy resin (NER-814) and were cut into 80 and 300-nm-thick thin slices with a microtome (ULTRACUT S) for the TEM and optical microscopic observations, respectively. The TEM images of the slices of (*S,S*)-**MS**$_{\mathbf{f2\text{-}f5}}$ showed either ellipsoidal or circular stripes, which were assignable to the longitudinal and horizontal cross-sections of the TB phase, respectively (Fig. 2k–l, o–p, s–t, w–x). The slices with the circular pattern in the TEM images were further observed by POM (Fig. S8a). The sliced **MS** showed Maltese cross at the periphery, while its interior remained dark regardless of the in-plane rotation.

We also observed the polarization of the fluorescence from the same slice by introducing an analyzer into FM and excited the sliced piece of **MS** with unpolarized light (Fig. 3a, b). The polarization of the fluorescence was dominant along the tangential direction of the circumference of the sliced **MS** (Fig. 3a). Analogously, the slices exhibiting elliptical pattern in TEM were observed with POM and polarized FM (Figs. 3b and S8b). The central elliptical band appeared bright in polarized FM, and its brightness altered periodically upon in-plane rotation (Fig. 3b). The dominant polarization from the central elliptical band was parallel to the long axis of the ellipsoid. All these images consistently proved the TB molecular order, where the main chain of PFBT aligned parallel to the direction of the topological poles at the core of **MS**, while, at the periphery of **MS**, PFBT radially developed cholesteric order with their helical axis parallel to the equator plane. We also confirmed the consistent bipolar structure with the non-sliced pristine **MS**s by observing the POM textures upon in- and out-of-plane rotation (Figs. S9–S14).

Microparticles with cholesteric molecular order is of particular interest regarding their high g_{lum} value. Accordingly, we measured CPL spectra of a MeOH suspension of (*S,S*)-**MS** and observed intense CPL with $|g_{\text{lum}}|$ as high as 0.15 (Fig. S15). We confirmed that CPL was not an artifact since the spectra obtained with (*R,R*)-**MS** exhibited a mirror-image CPL spectrum. Consistently, the spectra observed with achiral microspheres (a-**MS)** exhibited negligible CPL signals. We also confirmed that the luminescent intensities of **MS** were basically maintained for 20–30 min upon continuous optical pumping (Fig. S16).

The angle-dependent CPL measurements were performed with a homemade microscopy (Fig. S17)[22]. A single particle of **MS** was picked up with a sharp tungsten needle and set at the focal point of the microscope. A depolarized CW laser (λ_{ex} = 405 nm, spot size of 10 μm) was irradiated onto **MS** through an

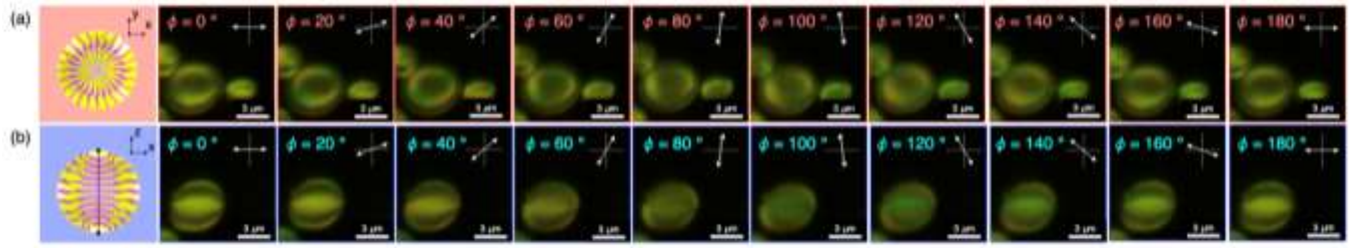

Fig. 3 (a,b) Schematic representation of the cross-sectional views of the TB molecular arrangement in **MS** and the polarization angle-dependent FL micrographs of a sliced (*S*,*S*)-$\mathbf{MS_{f3}}$ upon in-plane rotation of the analyzer.

objective lens, and PL was collected with another objective lens. The PL was transmitted through a quarter wave plate (QWP) and a subsequent linear polarizer (LP, Fig. S17) for separating the left- and right-handed CPL components at 546 nm (I_L and I_R). The measurements were conducted by rotating **MS** every 10° in the out-of-plane direction. The altitudinal angle θ was calculated by defining the equatorial plane as the origin and defining the zenith direction as 90°, which coincided with the direction of the topological defect. Experimentally, we observed **MS** with POM and defined θ as 90° when its POM texture appeared perfect spiral, which coincided with a direction of the topological defect.

The θ-dependent CPL intensities for **MS**s were summarized in Figure 4a and b. **MS** with the TB order ((*S*,*S*)-$\mathbf{MS_{f2–f5}}$) showed large $|g_{lum}|$ values that oscillated as a function θ with a period of 180°. The observed anisotropy is well coincided with that expected based on the TB molecular order. In contrast, (*S*,*S*)-$\mathbf{MS_{f1}}$ did not show any distinguishable CPL signal due to the absence of the TB order. The degree of angular anisotropy of g_{lum} ($r = (|g_{lum}^{max}| - |g_{lum}^{min}|) / (|g_{lum}^{max}| + |g_{lum}^{min}|)$, where g_{lum}^{max} and g_{lum}^{min} are the maximum and minimum values of g_{lum}, respectively, observed upon rotating the emitter) was evaluated based on the θ-dependent CPL intensities, and the values were plotted in Figure 4c. In definition, the r value approaches 1 with a perfectly anisotropic CPL emitters, while r approaches 0 with a fully isotropic CPL emitter. The $|g_{lum}^{max}|$ of (*S*,*S*)-$\mathbf{MS_{f2}}$ was 61-fold larger than its $|g_{lum}^{min}|$ (Fig. 4d) and yielded r of 0.95 on average (Fig. 4c and Table S1), which is the best anisotropy among minute CPL emitters reported previously by us and the other research groups. The large anisotropy was attributed to the very small $|g_{lum}|$ value at $\theta = 0$ and 180°, indicating that the cholesteric arrangement of PFBT align almost perfectly parallel to the equatorial plane. The large deviation of $|g_{lum}^{max}| / |g_{lum}^{min}|$ of $\mathbf{MS_{f2}}$ is due to the very small $|g_{lum}^{min}|$ value. In contrast, the $|g_{lum}|$ values of (*S*,*S*)-$\mathbf{MS_{f4,\ f5}}$ at θ = 0 and 180° were not suppressed significantly, leading to smaller r values (0.53 and 0.52), though they were still anisotropic in comparison to the typical CPL emitters. The relatively high $|g_{lum}|$ value at θ = 0 and 180° of $\mathbf{MS_{f3–f5}}$ in comparison to those of $\mathbf{MS_{f2}}$ indicates that some of the helices do not align parallel to the equatorial plane in $\mathbf{MS_{f3–f5}}$. The $|g_{lum}|$ value observed with $\mathbf{MS_{f4}}$ at θ = 90 and 270° was 0.73 on average and 0.93 at the highest, which is the largest among **MS** tested and is better than those observed previously[22] (Fig. S18).

The large $|g_{lum}|$ value observed herein is intrinsic to the molecular order in **MS** rather than an artifact due to linearly polarized luminescence or linear birefringence of the specimens[30]. We confirmed that the g_{lum} value was constant irrespective of the in-plane rotation (Fig. S19a), which is the direct experimental evidence of the absence of the artifact (Fig. S19b). We also eliminated the size effect by selecting **MS**s with nearly equal diameter (4–4.5 μm) for the optical measurements. The efficiencies of **MS**s to convert the absorbed light into CPL were also high due to the relatively high photoluminescence quantum yield of PFBT (Table S2).

As reported previously[22], PFBT formed lyotropic liquid crystalline phase during the formation of the spherical particles (Fig. S20). A question here is how the mesophase structure is

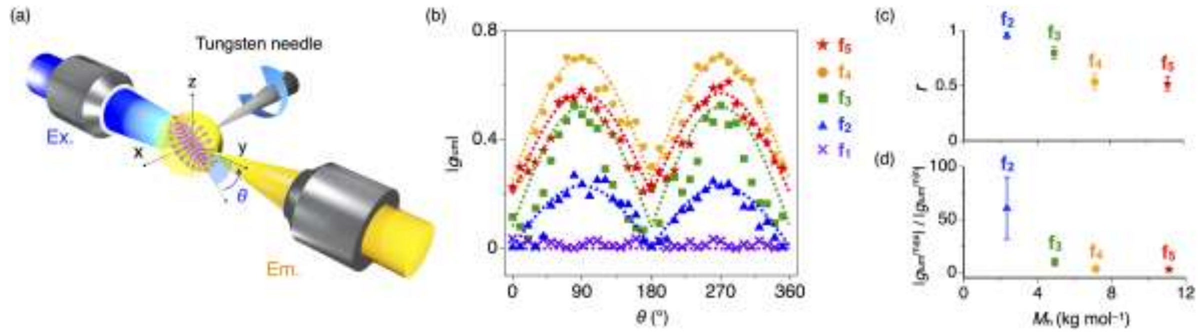

Fig. 4 (a) A schematic representation of the experimental setup for the angle-dependent CPL measurements with single particle of (*S*,*S*)-**MS**. (b) A plot of $|g_{lum}|$ at 546 nm as a function of θ (purple crosses: $\mathbf{MS_{f1}}$, blue triangles: $\mathbf{MS_{f2}}$, green squares: $\mathbf{MS_{f3}}$, orange circles: $\mathbf{MS_{f4}}$, and red stars: $\mathbf{MS_{f5}}$). Dotted curves are the fitted sine curves ($|g_{lum}| = a + b|\sin\theta|$). (c,d) Plots of r (c) and $|g_{lum}^{max}| / |g_{lum}^{min}|$ (d) as a function of M_n. Error bars represent standard deviation.

preserved throughout the solidification. For elucidating the thermal behaviour of the mesophase, we conducted differential scanning calorimetry with $\mathbf{f}_1$ to $\mathbf{f}_5$ (Fig. S21). Glass transition into mesophase was observed for $\mathbf{f}_1$–$\mathbf{f}_4$ and their transition temperature (T_g) decreased as decreasing M_n, indicating the superior stability of the mesophase for $\mathbf{f}_1$ and $\mathbf{f}_2$, which is preferable for the preservation of the molecular order upon solidification not only by cooling but also by de-solvation. Considering that $\mathbf{f}_1$ could not form discrete spheres efficiently, $\mathbf{f}_2$ should be the best fraction that can be assembled into microspheres and can facilitate the formation of the mesophase structure. Furthermore, the texture appeared upon heating was preserved even upon cooling below T_g (Fig. S22). We presumed that the same preservation process happened during the solidification of the lyotropic droplets into **MS**.

In summary, we succeeded in synthesizing a micrometre-scale spherical particles that emitted intense CPL in the equatorial plane while emitting non-biased CPL along the zenith axis, resulting in the degree of angular anisotropy as large as 0.97. The unprecedentedly high angular anisotropy was achieved by using a chiral conjugated polymer with an appropriate molecular weight and a narrow polydispersity index. This finding will contribute to the future materials chemistry aiming at synthesizing mesoscopic molecular assemblies with an intricate molecular order. The CPL properties expected from the resulting particles will surely pave the way for realizing advanced optical devices.

Data availability

The data supporting this article have been included as part of the Supplementary Information.

Conflicts of interest

There are no conflicts to declare.

Acknowledgements

The authors acknowledge Ms. Yuko Jinzenji for TEM observation of the slices of the microspheres and Dr. Takashi Nakamura for measuring photoluminescence quantum yield. This work was financially supported by CREST (JPMJCR20T4) from Japan Science and Technology Agency (JST), Grant-in-Aid for Scientific Research for Early-Career Scientists (JP22K14656) from Japan Society for the Promotion of Science (JSPS), and Kato Memorial Bioscience Foundation.

Notes and references

1. X. Zhan, F.-F. Xu, Z. Zhou, Y. Yan, J. Yao and Y. S. Zhao, *Adv. Mater.* 2021, **33**, 2104418.
2. F. Song, Z. Xu, Q. Zhang, Z. Zhao, H. Zhang, W. Zhao, Z. Qiu, C. Qi, H. Zhang, H. H. Y. Sung, I. D. Williams, J. W. Y. Lam, Z. Zhao, A. Qin, D. Ma and B. Z. Tang, *Adv. Funct. Mater.* 2018, **28**, 1800051.
3. Y. Dai, J. Chen, C. Zhao, L. Feng and X. Qu, *Angew. Chem. Int. Ed.* 2022, **61**, e202211822.
4. Q. Jiang, X. Xu, P.-A. Yin, K. Ma, Y. Zhen, P. Duan, Q. Peng, W.-Q. Chen and B. Ding, *J. Am. Chem. Soc.* 2019, **141**, 9490.
5. H. Wynberg, E. W. Meijer, J. C. Hummelen, H. P. J. M. Dekkers, P. H. Schippers and A. D. Carlon, *Nature* 1980, **286**, 641.
6. Q. Guo, M. Zhang, Z. Tong, Y. Zhou, Y. Wang, S. Jin, J. Zhang, H.-B. Yao, M. Zhu and T. Zhuang, *J. Am. Chem. Soc.* 2023, **145**, 4246.
7. H. Li, H. Li, W. Wang, Y. Tao, S. Wang, Q. Yang, Y. Jiang, C. Zheng, W. Huang and R. Chen, *Angew. Chem. Int. Ed.* 2020, **59**, 4756.
8. T. Goto, Y. Okazaki, M. Ueki, Y. Kuwabara, M. Takafuji, R. Oda and H. Ihara, *Angew. Chem. Int. Ed.* 2017, **56**, 2989.
9. N. Ryu, T. Kawaguchi, H. Yanagita, Y. Okazaki, T. Buffeteau, K. Yoshida, T. Shirosaki, S. Nagaoka, M. Takafuji, H. Ihara and R. Oda, *Chem. Commun.* 2020, **56**, 7241
10. P. Liu, Y. Battie, T. Kimura, Y. Okazaki, P. Pranee, H. Wang, E. Pouget, S. Nlate, T. Sagawa and R. Oda, *Nano Lett.* 2023, **23**, 3174.
11. D. D. Nuzzo, C. Kulkarni, B. Zhao, E. Smolinsky, F. Tassinari, S. C. J. Meskers, R. Naaman, E. W. Meijer and R. H. Friend, *ACS Nano* 2017, **11**, 12713.
12. D.-M. Lee, J.-W. Song, Y.-J. Lee, C.-J. Yu and J.-H. Kim, *Adv. Mater.* 2017, **29**, 1700907.
13. J. Crassous, M. J. Fuchter, D. E. Freedman, N. A. Kotov, J. Moon, M. C. Beard and S. Feldmann, *Nat. Rev. Mater.* 2023, **8**, 365.
14. L. Frédéric, A. Desmarchelier, L. Favereau and G. Pieters, *Adv. Funct. Mater.* 2021, **31**, 2010281.
15. J. Roose, B. Z. Tang and K. S. Wong, *Small,* 2016, **47**, 6495-6512.
16. Y. Deng, M. Wang, Y. Zhuang, S. Liu, W. Huang and Q. Zhao, *Light: Sci. Appl.* 2021, **10**, 76.
17. Y. Sang, J. Han, T. Zhao, P. Duan and M. Liu, *Adv. Mater.* 2020, **32**, 1900110.
18. K. Watanabe, H. Iida and K. Akagi, *Adv. Mater.* 2012, **24**, 6451.
19. J. He, S. Liu, G. Gao, M. Sakai, M. Hara, Y. Nakamura, H. Kishida, T. Seki and Y. Takeoka, *Adv. Opt. Mater.* 2023, 2300296.
20. A. P. Gardymova, M. N. Krakhalev and V. Y. Zyryanov, *Molecules* 2020, **25**, 1740.
21. J. Jeong, Z. S. Davidson, P. J. Collings, T. C. Lubensky and A. G. Yodh, *Proc. Natl. Acad. Sci. USA* 2014, **111**, 1742.
22. O. Oki, C. Kulkarni, H. Yamagishi, S. C. J. Meskers, Z.-H. Lin, J.-S. Huang, E. W. Meijer and Y. yamamoto, *J. Am. Chem. Soc.* 2021, **143**, 8772.
23. N. Nishizawa, B. Al-Qadi and T. Kuchimaru, *J. Biophotonics* 2021, **14**, e202000380
24. H.-G. Kuball and T. Höfer, *Chirality* 2000, **12**, 278.
25. R. Abbel, A. P. H. J. Schenning and E. W. Meijer, *Macromolecules* 2008, **41**, 7497.
26. T. Adachi, L. Tong, J. Kuwabara, T. Kanbara, A. Saeki, S. Seki and Y. Yamamoto, *J. Am. Chem. Soc.* 2013, **135**, 870 .
27. D. Okada, T. Nakamura, D. Braam, T. D. Dao, S. Ishii, T. Nagao, A. Lorke, T. Nabeshima and Y. Yamamoto, *ACS Nano* 2016, **10**, 7058.
28. S. Kushida, S. Okabe, T. D. Dao, S. Ishii, T. Nagao, A. Saeki, M. Kijima and Y. Yamamoto, *RSC Adv.*, 2016, **6**, 52854.
29. S. Kushida, D. Braam, T. D. Dao, H. Saito, K. Shibasaki, S. Ishii, T. Nagao, A. Saeki, J. Kuwabara, T. Kanbara, M. Kijima, A. Lorke and Y. Yamamoto, *ACS Nano* 2016, **10**, 5543.
30. T. Harada, R. Kuroda and H. Moriyama, *Chem. Phys. Lett.* 2012, **530**, 126.